Proceedings of International Conference on Heat Exchanger Fouling and Cleaning - 2015 (Peer-reviewed)
June 07 - 12, 2015, Enfield (Dublin), Ireland
Editors: M.R. Malayeri, H. Müller-Steinhagen and A.P. Watkinson
Published online
www.heatexchanger-fouling.com

VALUE PRICING OF ANTIFOULING COATINGS IN HEAT EXCHANGERS

O.M. Magens[1], J. Hofmans[2], M. Pabon[3] and D.I. Wilson[1*]

[1] Department of Chemical Engineering and Biotechnology, University of Cambridge, Cambridge, CB2 3RA, UK
[2]Chemours/DuPont de Nemours BVBA, A. Spinoystraat 6A, B-2800 Mechelen, Belgium
[3]Chemours/DuPont de Nemours International S.A., 2, Chemin du Pavillon, PO Box 50, CH-1218 Le Grand-Saconnex, Geneva, Switzerland
* Corresponding author. Email: diw11@cam.ac.uk; Tel. +44(0) 1223 334 777; Fax. + 44(0) 1223 334 796

ABSTRACT

Fouling reduces the thermal and hydraulic performance of heat exchangers over time, requiring regular cleaning. A wide range of anti-fouling coatings has been proposed, but attempts have only recently been made to quantify their financial attractiveness rigorously. Whether or not it is attractive to install a coated exchanger depends on trade-offs between capital and operating costs over the lifetime of the unit. The techno-economic 'value pricing' analysis of coating performance introduced by Gomes da Cruz *et al.* (2015) is applied here to a heat exchanger with more realistic heat transfer and fouling performance, specifically distributed temperatures and temperature sensitive fouling rates. Calcium carbonate crystallisation fouling is modelled using the surface growth model and parameters reported by Pääkkönen *et al.* (2015). The performance of coatings are compared with the uncoated case and the envelope where a coating is financially attractive is identified. The data needed to perform these calculations are discussed.

INTRODUCTION

Fouling deposits on heat transfer surfaces reduce the thermal and hydraulic performance of heat transfer equipment over time. Deposits which grow and detach can, moreover, lead to blockage, as well as compromising hygienic operation and product quality if the processed streams are functional materials (*e.g.* food, pharmaceuticals, fine chemicals). This gives rise to the need to clean heat exchangers on a regular basis. Cleaning actions are not instantaneous, requiring the unit to be taken out of service. Cleaning incurs further heat transfer losses, or capital expenditure to provide a backup facility to substitute for the absent unit.

Antifouling coatings should extend the operating period before cleaning is required, and/or improve cleaning rates or effectiveness: the financial benefit of this needs to be balanced against the cost of installing a new or revamped unit. This is the core of the 'value pricing' concept introduced by Gomes da Cruz *et al.* (2015) and involves a series of modelling and optimisation calculations.

The decision when and how to clean a fouling heat exchanger is an optimisation problem, first considered by Ma and Epstein (1981). Fig. 1 illustrates the underlying problem for a single heat exchanger. Operation for a period of length t incurs an amount of energy loss. Cleaning restores the heat duty, Q, to the clean state, Q_{cl}. However, cleaning requires the unit to be taken offline for time τ, and induces further costs for the cleaning operation, C_{cl}.

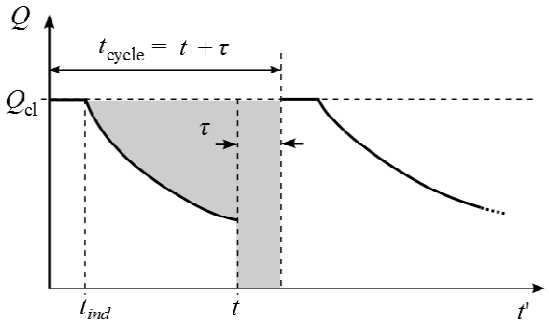

Fig. 1 Schematic of the fouling-cleaning cycle in a single heat exchanger over time t'. Following an induction period with negligible deposition of length t_{ind}, the duty Q falls from the clean value Q_{cl}. After operating for time t the unit is cleaned, taking time τ, and performance is restored to Q_{cl}. Grey shaded area represents energy lost (after Magens *et al.*, 2015)

The objective function to be optimized is the time-averaged operating cost, ϕ_{op}, calculated thus:

$$\phi_{op} = \frac{c_E\left[\int_0^t \left(Q_{cl} - Q(t')\right)dt' + Q_{cl}\tau\right] + C_{cl}}{t+\tau} \quad (1)$$

where c_E is the cost per unit energy. The optimal processing period, t_{opt}, is found by setting $d\phi_{op}/dt = 0$, which yields

$$\phi_{op}(t_{opt}) = c_E\left(Q_{cl} - Q(t_{opt})\right) \quad (2)$$

Furthermore, the condition for a minimum in ϕ_{op} to exist, $d^2\phi_{op}/dt^2 > 0$, requires the heat duty to decline: $dQ/dt < 0$. Computation of the operating cost requires knowledge of the fouling behaviour over time, $Q(t')$. If this is available, it allows the operator or designer to determine the optimal operating strategy and configuration of a heat exchanger.

Gomes da Cruz (2015) considered the linear fouling case, where the fouling resistance, R_f, increases at a constant rate. They quantified the attractiveness of anti-fouling coatings to mitigate fouling using a techno-economic analysis of the optimal operating performance of an individual heat exchanger and compared this with the cost of installation of a coated unit. The upper price that can be charged for a coating is set by its ability to reduce deposition and enhance cleaning, while the lower limit is set by manufacturing costs. Quantifying this price range, wherein value is created for the vendor and purchaser, should ideally be performed early in the decision process as it helps to set targets for the coating performance as well as manufacturing cost.

Magens *et al.* (2015) extended the above approach to consider asymptotic fouling behaviour, which is more common. They presented analytical solutions for the case where the heat exchanger could be modelled using lumped model methods. This paper extends their work further by considering spatially and temporally dynamic fouling behaviour. Changes in the processing conditions and the conditions at the heat transfer interface influence the local fouling rate and cause predictions from lumped models to be inaccurate, which in turn affects ϕ_{op}. Geddert *et al.* (2009) identified processing conditions influencing fouling as including the nature and source of the foulant, additives, bulk temperature, flow velocity and flow regime. The local surface temperature, its surface energy, roughness, topography and number of nucleation sites (particularly for crystallization fouling) are also important.

Coatings to mitigate fouling (increase Q) and/or enhance cleaning (decrease τ and C_{cl}) are the subject of much effort in industry and academia. Gomes da Cruz *et al.* (2015) reviewed the different methods for coating heat transfer surfaces with anti-fouling properties, often by manipulating surface energy and adhesion. From the heat transfer perspective, coatings can be classified as those which impose extra thermal resistance and those with negligible impact on heat transfer. For example, fluorocarbon-based polymer surfaces provide low surface energies, but tend to have low thermal conductivity (Zhao *et al.*, 2002). Considerable effort has been spent on improving their abrasion resistance and adhesion to the substrate. Their non-stick properties have set the benchmark in household applications and are effective even after years of harsh thermal conditions and cleaning procedures. An idealised fluorocarbon coating is considered here.

SPATIALLY DISTRIBUTED MODEL

The temperature distribution within a single pass counter-current heat exchanger is calculated over time. A local crystallisation fouling model sensitive to processing and interface conditions is incorporated using the approach presented by Fryer and Slater (1985). More complex simulations such as that reported by Coletti *et al.* (2010) could be used, if desired. Similarly, other types of fouling could implemented (Fryer and Slater studied chemical reaction fouling by milk).

Figure 2 shows a differential element of area of the heat exchanger: $dA = A\delta z/L$. Enthalpy balances on the hot and cold streams yield the following constitutive partial differential equations for the (well-mixed) bulk fluid temperatures at axial position, z, and time, t':

Hot side fluid $T_h(t', z)$

$$\frac{\partial T_h}{\partial t'} = -\frac{UAv_h}{LW_h}\left(T_h - T_c\right) + v_h \frac{\partial T_h}{\partial z} \tag{3}$$

Cold side fluid $T_c(t', z)$

$$\frac{\partial T_c}{\partial t'} = \frac{UAv_c}{LW_c}\left(T_h - T_c\right) - v_c \frac{\partial T_c}{\partial z} \tag{4}$$

Here, U is the local overall heat transfer coefficient, A is the total heat transfer area, v_c and v_h are the local bulk fluid velocities, L is the length of the unit and W_c and W_h are the heat capacity flow rates. U includes the film heat transfer coefficients, the wall and any fouling resistances.

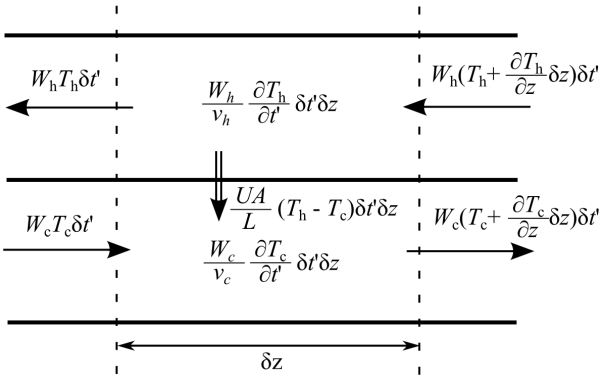

Fig. 2 Elements of the enthalpy balance on either side of an increment of length for a countercurrent heat exchanger (after Fryer and Slater, 1985).

Both streams are aqueous. Water property variation with temperature is interpolated from the VDI database (VDI, 2010). This approach allows the local deposit interface temperature and transport coefficients to be evaluated and changes with time accounted for.

CRYSTALLISATION FOULING MODEL

The cold stream is assumed to contain dissolved calcium carbonate which causes crystallization fouling. Solubility is a function of the conditions at the location of crystal formation, in particular the temperature (Bott, 1997). The effects of pH, pressure and the presence of other chemical species are not considered here but could be included if desired. Assuming the solid phase to be calcite, the solubility, C_s (in kg/m^3), at the deposit-solution interface temperature, T_i, is calculated using the correlation reported by Pääkkönen *et al.* (2015) (where T_i is in °C).

$$C_s = -379.33\cdot10^{-10}T_i^{\,3} + 128.11\cdot10^{-7}T_i^{\,2} - 167.15\cdot10^{-5}T_i + 122.11\cdot10^{-3} \tag{5}$$

Aragonite and vaterite have higher solubilities and are not expected to participate (Helalizadeh *et al.*, 2000). The temperature distribution and flow conditions are assumed to

favour surface integration controlled deposition (Bott, 1997; Bansal *et al.*, 2008) The integration step is a complicated process, involving the physics of heterogeneous nucleation, chemistry of the solid-liquid interface and local thermo- and hydrodynamics (Pääkkönen *et al.*, 2015). Rather than modelling all these processes in detail, the rate of deposition into the crystal lattice is calculated *via.*

$$\frac{dm_f}{dt'} = k_d' \exp\left(\frac{-E_a}{RT_i}\right)(C_i - C_s)^j \tag{6}$$

with the dependency on the difference between the saturation concentration, C_s, and the concentration at the interface, C_i, being set as $j = 2$ (Helalizadeh *et al.*, 2000; Mwaba *et al.*, 2006; Bansal *et al.*, 2008; Pääkkönen *et al.*, 2015). E_a is the activation energy and R the gas constant. If the integration step controls fouling, the concentration of species at the wall, C_i, is practically equal to the bulk concentration, C_c. The interface temperature is calculated using the internal film heat transfer coefficient, h_c, *via.*

$$T_i = \frac{U}{h_c}(T_h - T_c) + T_c \tag{7}$$

The deposition rate factor, k_d', is expected to be a function of local flow velocity or residence time. The sticking factor formulation suggested by Epstein (1994) is used: $k_d' = k_d \mu_l/(\rho_l V^2)$, where μ_l denotes the viscosity of the liquid and ρ_l is the liquid density evaluated at interface temperature. V is the friction velocity, estimated using the Blasius correlation

$$V = \sqrt{\frac{\tau_i}{\rho}} = v_c\sqrt{\frac{f}{2}} = v_c\sqrt{\frac{0.0791}{2\mathrm{Re}^{0.25}}} \tag{8}$$

Here, τ_i is the shear stress imposed on the fouling layer and *Re* is the Reynolds number of the cold stream evaluated at the interface temperature. Incorporation of additional material into the deposit becomes more difficult as the crystal layer grows and long crystals are likely to be less robust against removal forces (Bott, 1997). A suppression or term could be included to address this, but is neglected here.

The fouling layer is assumed to be homogeneous and fouling slow, so that the bulk concentration of fouling precursors does not change with z. The local fouling resistance is calculated from $R_f = m_f/(\rho_f k_f)$ and the fouling Biot number is given by $Bi_f = R_f U_{cl}$. The local duct diameter changes as a result of layer growth (thickness $\delta_f = m_f/\rho_f$) so T_i, V, C_s and fluid properties vary with position and time. Hence the fouling rate and Bi_f vary as $f(z, t')$.

SOLUTION METHOD

Fryer and Slater (1985) used the method of characteristics to convert the hyperbolic partial differential equations (3) and (4) into ordinary differential equations. The characteristic lines associated with the convectional enthalpy transport, with velocities v_c and v_h, constrain the numerical integration to a distinct step size, which proves to be the largest satisfying the Courant-Friedrichs-Lewy criterion for the two stiff equations when using an explicit integration method (Press, 1986). Fryer and Slater were interested in fast fouling, reaching an asymptote in about one hour. For slower fouling rates with a high spatial resolution, multistep methods such as those in Matlab® ode15s, are more efficient and are used here.

Equations (3) and (4) are integrated numerically over time. The spatial derivatives are approximated with a first order upwind scheme and finite Δz, giving for the hot stream

$$\frac{\partial}{\partial z}T_h(t', z) \approx \frac{T_h(t', z+\Delta z) - T_h(t', z)}{\Delta z} \tag{9}$$

and for the cold stream

$$\frac{\partial}{\partial z}T_c(t', z) \approx \frac{T_c(t', z) - T_c(t', z-\Delta z)}{\Delta z} \tag{10}$$

This upwind scheme is preferred over central differencing schemes since advective enthalpy transfer dominates diffusive transfer and heat can only propagate in the direction of bulk flow. The continuous coordinates, t' and z, are discretized with a mesh of temporal, $k = 1, 2\ldots K$, and spatial, $n = 1, 2\ldots N$, nodes. Figure 3 shows a schematic of the spatial mesh. N, was set at 150, as larger values gave no appreciable increase in accuracy.

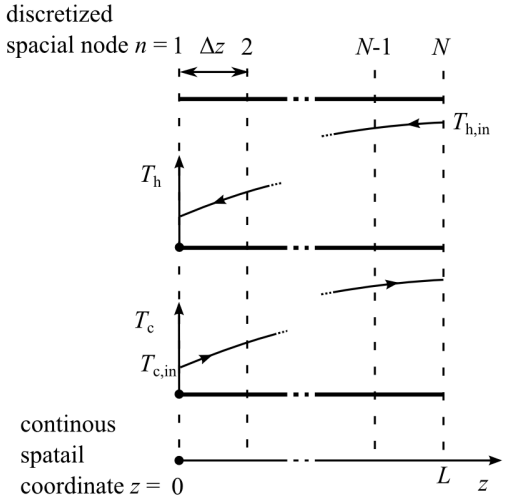

Fig. 3 Scheme of the spatial mesh of the exchanger. N nodes are equally spaced along the physical length L.

Cleaning is assumed to remove all fouling. The initial temperatures of all nodes n at $k = 0$ are set to the steady state profile for the clean exchanger, obtained by running an initial simulation fouling, *i.e.* $dm_d/dt' = 0$. The temperatures converge rapidly to the clean distribution. This was verified by comparison with analytical results.

To define upwind derivatives at the inlet boundaries, $T_h(k, N+1)$ and $T_c(k, 0)$ are arbitrarily set to zero. This is a computational measure as the unit operates with constant inlet temperatures. The boundary conditions

$$T_h(t', z) = T_{hin} \quad z = L, \forall t' \tag{11}$$

$$T_c(t', z) = T_{cin} \quad z = 0, \forall t' \tag{12}$$

are enforced by setting the numerical temporal derivatives at each inlet to zero, *i.e.*

$$\frac{\partial T_h(k, N)}{\partial t'} = \frac{\partial T_c(k,1)}{\partial t'} = 0 \tag{13}$$

CRYSTALLIZATION FOULING CASE STUDY

Pääkkönen *et al.* (2015) studied scaling of $CaCO_3$ on a flat-plate AISI 316L stainless steel heat exchanger surface and measured initial mass deposition rates under transitional and turbulent flow conditions. No induction period was observed and they reported that Equation (6) gave closest agreement with their data. The kinetic parameters, experimental conditions and properties of the porous fouling layer are given in Table 1. The fouling model described above was verified against Pääkkönen *et al.*'s results.

Table 1: Kinetic parameters, experimental conditions and fouling layer properties (after Pääkkönen *et al.*, 2015).

Kinetic parameters		
k_d	Deposition rate factor	$1.62 \cdot 10^{20}$ m^4/kg s^2
E_a	Activation energy	148 000 J/mol
Operating conditions		
T_i	Interface temperatures	332 – 358 K
C_c	$CaCO_3$ concentration	0.418 kg/m^3
D_{hyd}	Hydraulic diameter	0.03 m
v	Bulk velocities	0.18 – 0.35 m/s
Re	Reynolds number (parallel plates)	6000 – 12000
Fouling layer properties		
ρ_f	Density	971 ± 13 kg/m^3
k_f	Thermal conductivity	0.66 ± 0.011 W/m K

We illustrate value pricing of antifouling coatings by comparing an uncoated stainless steel and a polymer coated single-pass counter-current shell-and-tube heat exchanger operating at constant flow rates and inlet temperatures. The coating introduces an additional thermal resistance to the overall heat transfer coefficient, which is evaluated using

$$U = \left(\frac{1}{h_c} + \frac{Bi_f}{U_{cl}} + \frac{\delta_{coat}}{k_{coat}} + \frac{r_c}{k_{wall}} \log\left(\frac{r_h}{r_c}\right) + \frac{r_c}{r_h h_h} \right)^{-1} \tag{14}$$

where r_c and r_h are the internal and external radii of the tubes, h_c is the internal and h_h the external film heat transfer coefficient, δ_{coat} the coating thickness, and k_{coat} and k_{wall} are the coating and tube wall thermal conductivities, respectively. Baffles are not considered and the flow in the shell is assumed to be parallel to the tubes. The film heat transfer coefficients are estimated using the Gnielinski correlation with temperature dependent water properties and the approporiate hydraulic diameters (Bergman *et al.*, 2011).

The difference in U values means that the coated unit requires a larger heat transfer area to achieve the specified clean heat duty. This is calculated from the number of transfer units, *i.e.* $A_{coat} = AU_{cl}/U_{cl,coat}$ and the length of the coated exchanger increased accordingly. For the uncoated unit, δ_{coat} is zero. The design and operating parameters of the two heat exchangers are summarised in Table 2.

Operating conditions were selected to be initially comparable to the conditions in the Pääkkönen *et al.* (2015) experiments. The fouling model (6) is solved together with the enthalpy balances (3) and (4) in Matlab® on a desktop PC. As the fouling layer builds up, the increase in fluid velocities, caused by decreasing duct diameter, reduces the fouling rate significantly.

Table 2: Design, operating and cost parameters of the coated and uncoated (unc) heat exchangers.

Design of the uncoated unit		
A	Heat transfer area	96.7 m^2
L	Length	20.0 m
NT	Number of tubes	150
r_c	Inner tube radius	5.1 mm
r_h	Outer tube radius	6.4 mm
s	Tube spacing	9.1 mm
r_{shell}	Shell radius	103 mm
k_{wall}	Tube thermal conductivity	16 W/m K
U_{cl}	Overall clean heat transfer coefficient	234 W/m^2 K
Q_{cl}	Clean heat duty	482 kW
Modified design of the coated unit		
k_{coat}	Coating thermal conductivity[1]	0.1 W/m K
δ_{coat}	Coating thickness[1]	10 µm
A_{coat}	Heat transfer area	99.0 m^2
L_{coat}	Length	20.5 m
$U_{cl,coat}$	Overall clean heat transfer coefficient	229 W/m^2 K
Operation		
w_c	Cold stream mass flow	4 kg/s
w_h	Hot stream mass flow	4 kg/s
$T_{h,in}$	Hot stream inlet temperature	363.15 K
$T_{c,in}$	Cold stream inlet temperature	313.15 K
C_c	$CaCO_3$ concentration	0.418 kg/m^3
τ	Time taken for cleaning	3 days
v_c	Cold stream bulk velocity, unc	0.32 – 2.8 m/s
Re_c	Cold Reynolds number, unc	5000 – 22000
Costs		
c_E	Cost per unit heat	$57 \cdot 10^{-10}$ US$/J
C_{cl}	Cleaning cost per unit	2000 US$
t_{lf}	Asset lifetime (depreciation)	5, 10, 15 years

[1] Data taken from Gomes da Cruz *et al.*, 2015

RESULTS AND DISCUSSION

Figure 4 shows the temperature distribution in the uncoated exchanger at different times. The change in temperatures of both streams across the exchanger becomes smaller with time owing to fouling. There is little change in

the cold stream temperature distribution near its inlet as there is less deposition here as the level of supersaturation, which drives crystallisation (Equation (6)) is smaller. In the second half of the exchanger there is noticeable change over time as this is where fouling, driven by bulk temperature and saturation, is highest for the inverse solubility salt.

Figure 5 shows the distribution of deposit in the uncoated exchanger at different times, expressed as the local fouling Biot number. The Biot number at the hot end exceeds 1 at extended time, indicating a significant change in U. The fouling layer formation kinetics are not trivial as a result of the dynamic interdependency between heat transfer and temperature sensitivities in the fouling model.

There is a noticeable transition from convex to concave fouling distributions over time, and autoretardation at the hot end. As the fouling layer grows, interface temperatures decrease. Duct narrowing causes the flow velocity to increase, resulting in a lower fouling rate. Ishiyama *et. al.* (2008) presented a technique to calculate the mean fouling rates in co- and counter-current heat exchangers assuming a linear change in temperature across the unit. They also assumed that the fouling layer thickness does not vary considerably over the tube length: so fouling rates tended to increase monotonically across the unit. Figures 4 and 5 show that their approach would not be applicable to this case. The cold temperature profile is initially linear but becomes non-linear over time. Figure 5 shows evidence of strong variations in local fouling rate, generated by different sensitivities to interface and bulk temperature in the Arrhenius rate constant and the solubility in Equation (6). After long periods of time, it has to be expected that the interface temperature, and hence the fouling layer thickness, becomes more and more uniform.

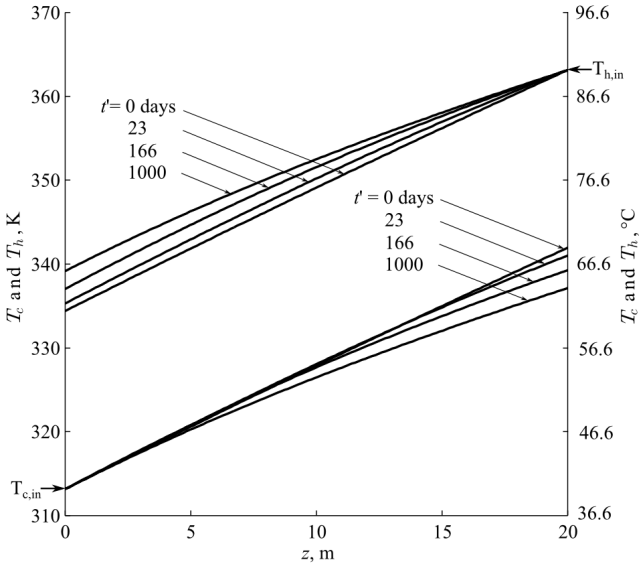

Fig. 4 Bulk temperature distribution along the uncoated heat exchanger at different times, t'.

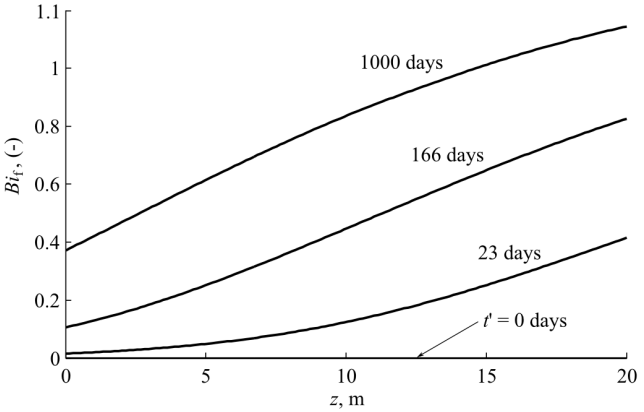

Fig. 5 Fouling Biot number distribution in uncoated exchanger at selected times, t'.

The effect of fouling on the overall fouling resistance for the uncoated unit is presented in Figure 6. The overall trend could be described as falling rate fouling and arises from two autoretardation mechanisms, namely decreasing T_i and changes in sticking factor. This will be accompanied by an increase in cold stream pressure drop. Asymptotic fouling behaviour as reported by Zhao *et al.* (2002) for $CaSO_4$ fouling on a stainless steel surface, would require a suppression or removal term.

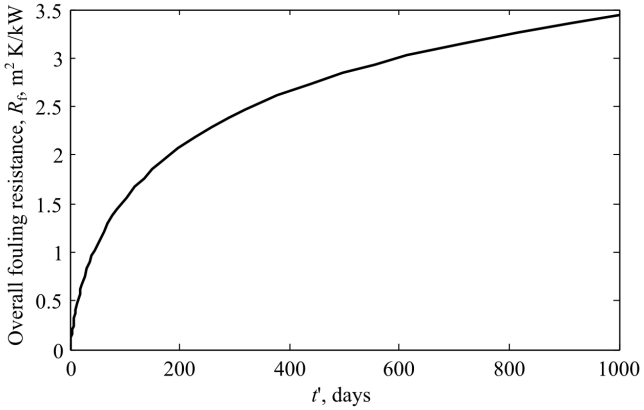

Fig. 6 Evolution of the overall fouling resistance, R_f, of the uncoated unit.

The impact of fouling on financial performance is plotted in Figure 7. The optimal processing period, t_{opt}, is reached after 316 days of processing, when the operating cost, ϕ_{op}, calculated with Equation (1), equals the thermal cost of fouling. At t_{opt} = 316 days, the overall fouling resistance is 2.5 m^2 K/kW, which corresponds to a mean fouling layer thickness of $\delta_f \simeq R_f\ k_f$ = 1.65 mm. This is significant compared to the tube radius of 5.1 mm, such that approximating the fouling layer as a thin slab is not accurate. If deposits of this thickness were encountered regularly, the assumptions in deriving Equation (14) would need to be revised.

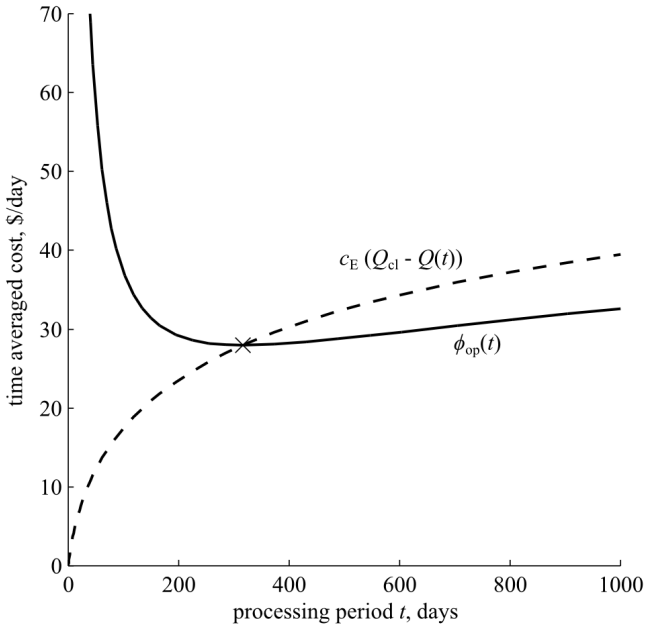

Fig. 7 Effect of processing period length, t, on the annualised operating cost, ϕ_{op}, and the thermal cost of fouling for the uncoated heat exchanger. The cross (at t_{opt} = 316 days, $\phi_{op,opt}$ = 27.96 $/day) indicates where Equation (2) is satisfied.

Pääkkönen *et al.* (2015) only studied calcite deposition on stainless steel so the antifouling performance of a series of fictitious coatings is examined here in a sensitivity analysis. The parameters of the fouling model are varied to represent improved fouling characteristics:

(*i*) Geddert *et al.* (2009) looked at fouling on modified surfaces at higher Reynolds numbers and reported that the deposition rate constant was smaller for surface modifications with anti-fouling properties. This is investigated by specifying the ratio of deposition rate constants, in the range 0.1 (good antifouling) ≤ $k_{d,coat}/k_d$ ≤ 1 (no benefit). The lower limit can be chosen as needed: if $k_{d,coat}$ = 0 there is no need to clean!

(*ii*) Mayer *et al.* (2012) found that anti-fouling surfaces exhibited lower adhesion forces between $CaCO_3$ crystals and surfaces, which is likely to facilitate cleaning. This would primarily reduce the time taken for cleaning, τ, and is investigated for 0.1 ≤ τ_{coat}/τ ≤ 1.

(*iii*) A coating providing fewer nucleation sites and with surface energy hindering heterogeneous nucleation is expected to promote longer induction periods at low flow velocities. However, reliable prediction of induction periods is difficult so is not considered here (see Gomes da Cruz, 2015, for examples). Since the crystallisation mechanism is unaffected by the coating after an initial crystal layer is formed, the activation energy, E_a, is unlikely to be affected.

The coated heat exchanger is presumed to be operated for the optimum processing period, then cleaned. Fig. 8 shows the effect of different levels of coating performance (deposition rate and cleaning time) on the dimensionless optimal operating cost, calculated by reference to the performance of the uncoated exchanger in Figure 7. In general, a decrease in time required for cleaning has a limited effect on the operating cost as the operating periods are very long: this is evident from Equation (1) if τ is small compared to t_{opt}. A reduction in deposition rate constant, gives an appreciable difference in operating cost. This provides guidance for the development of coatings, since innovations in other contexts often show a diminishing marginal benefit. In this case the induction period would have to be long, in order to influence ϕ_{op} significantly.

Not shown in Figure 8 is the associated value of t_{opt}, which will be longer than 316 days. This also constitutes important guidance as the coating must maintain its integrity (e.g. not spall off) and performance over the extended period if it is to be considered for use in practice. Alternatively, these calculations can provide indications of the minimum life expectancy required of such coatings.

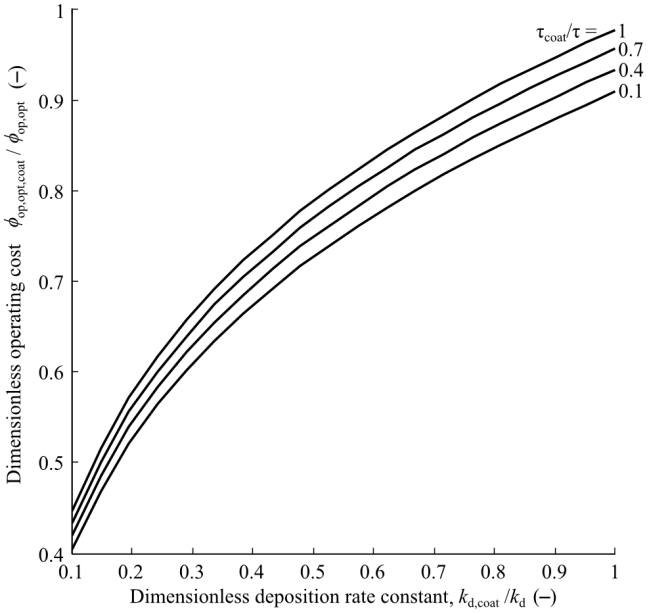

Fig. 8 Effect of antifouling coating performance (deposition rate and cleaning time) on the ratio of optimal operating cost to that of the uncoated exchanger.

Capital costs are now considered. A coated exchanger could be considered to replace an existing unit, in a revamp or retrofit, or as an alternative to an uncoated unit for a new plant. The latter, greenfield, scenario, is considered here. Excluding the cost of the coating, the capital cost of the base unit, C_{cap}, is calculated as an amortised cost, $\phi_{cap} = C_{cap}/ t_{lf}$, assuming straight line depreciation over the unit (or coating) lifetime, t_{lf}. Other depreciation policies could be considered, depending on the accounting practice to be used. The total optimised annualised cost is then $\phi_T = \phi_{cap} + \phi_{op,opt}$.

According to Hewitt *et al.* (2007), a 100 m^2 carbon steel TEMA BEM type heat exchanger cost approximately 140 GBP/m^2 in 1994. Conversion into US$ and updating it with the chemical engineering plant index to December 2013 yields an installed cost of 332 US$/m^2. Taking this cost as an estimate and assuming 10 years asset lifetime, the

amortised capital costs of the base units are ϕ_{cap} = 35.14 US$/day for the uncoated unit and $\phi_{cap,coat}$ = 35.97 US$/day for the slightly larger coated unit, before coating costs are added. Müller-Steinhagen *et al.* (1997) stated the low thermal conductivity of polymers such as PTFE was one of the main disadvantages of polymer based anti-fouling coatings in heat exchangers. This does not hold true for this case, possibly because the coating is thin. Given that ϕ_{op} is approximately 28 US$/day for the uncoated unit, the contribution from capital expenditure is modest: techno-economic analysis suggests that the heat transfer penalty is negligible in comparison to the potential savings when processing streams prone to serious fouling. The maximum price for coating such an exchanger can be calculated from

$$c_{coat,\max,new} = \left(\phi_T - \phi_{T,coat}\right) t_{lf} \,/\, A_{coat} \tag{15}$$

This is the 'value price' for coating a heat exchanger to mitigate fouling. It represents the maximum benefit arising from installing the coated item, to be shared between the operator and the coating vendor. If the coating cannot be provided at this price or less there is no incentive for the operator to consider it. Figure 9 shows a map of potential value prices calculated for the cases in Figure 8. Neither inflation nor the time value of money is considered here, but could be introduced to calculate the net present value.

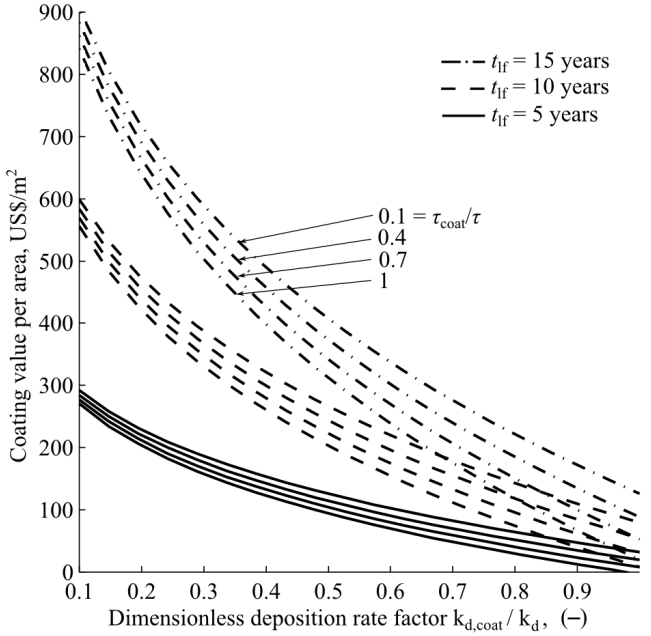

Fig. 9 Value prices of coating for different ratios of deposition rates, three asset lifetimes, and four dimensionless cleaning period lengths.

The strong effect of asset lifetime, t_{lf}, is evident in the results in Figure 9. In practice, the asset lifetime is likely to be limited by the coating's durability. Assuming the coating is stable and retains its effectiveness, it creates maximum value if it prevents fouling completely. Zhao *et al.* (2002) conducted fouling experiments with aqueous $CaSO_4$ solution on stainless steel surfaces. While crystal deposits on the stainless steel surface resulted in a 38% lower heat transfer coefficient, a parallel experiment with a nickel–phosphorus/PTFE coating exhibited no fouling over the duration of the experiment. If this most promising result would apply to the current case, the coating value would greater than 300 – 900 US$/m^2, depending on t_{lf}.

Fluoropolymers generally provide good corrosion resistance so a fluoropolymer coated carbon steel unit could be considered as an alternative to a stainless steel unit. Carbon steel is cheaper and conducts heat better than the stainless variety: this could compensate for the additional thermal resistance imparted by the coating. Gomes da Cruz *et al.* (2015) investigated this scenario and showed it to be an attractive option. The coating again has to be stable and impermeable for the whole time in service.

CONCLUSIONS

1. The enthalpy balances of a pure counter-current heat exchanger were solved together with a fouling model to predict the heat duty and fouling dynamics in a simple heat exchanger subject to crystallisation fouling.
2. The heat exchanger model was able to demonstrate non-linear fouling dynamics arising from different temperature dependencies in crystallisation fouling.
3. A methodology for assessing the economic value of specific coatings was demonstrated for various combinations of antifouling effectiveness.
4. For the case study considered, a shorter cleaning period had a substantial, but limited effect on the operating cost compared to the thermal savings when reducing the deposition rate factor.
5. The low thermal conductivity of the polymer coating considered here had negligible effect compared to the potential gain from fouling mitigation.

ACKNOLEDGEMENTS

A PhD studentship for OMM from Du Pont/Chemours is gratefully acknowledged.

NOMENCLATURE

A heat transfer area (m^2)
Bi_f fouling Biot number (–)
C $CaCO_3$ concentration (kg/m^3)
C_{cap} capital cost of the base unit (US$)
C_{cl} cleaning cost per heat exchanger unit (US$)
c_{coat} coating price per area (US$/m^2)
c_E cost per unit heat (US$/J)
D_{hyd} hydraulic diameter (m)
E_a activation energy (J/mol)
f fanning friction factor (–)
h film heat transfer coefficient (W/m^2 K)
j order of the crystal integration reaction (–)
K total number of temporal nodes
k thermal conductivity (W/m K)
or temporal node 0,1,…k…K (–)
k_d deposition rate factor (m^4/kg s^2)
k_d' deposition rate factor $k_d' = k_d \mu_l/(\rho_l V^2)$ (m^4/kg s)
L length of the heat exchanger (m)
m_f mass of the fouling layer per covered area (kg/m^2)

N total number of spatial nodes (–)
NT number of tubes (–)
n spatial node 0,1,…n…N (–)
Q heat duty (kW)
R gas constant (J/mol K)
Re Reynolds number (–)
R_f fouling resistance (m^2 K/W)
r radius (mm)
s tube spacing (mm)
t operating period (days)
t_{lf} asset lifetime (years)
t' time, used as variable in integrand $0 \le t' \le t$ (days)
T temperature (K)
U heat transfer coefficient (W/m^2 K)
V friction velocity (m/s)
v bulk fluid velocity (m/s)
W heat capacity flow rate (J/s K)
w mass flow rate (kg/s)
z position along the exchanger $0 \le z \le L$ (m)
Δz spatial step size (m)

δ thickness (m)
μ viscosity (Pa s)
ρ density (kg/m^3)
τ time taken for cleaning (days), shear stress (Pa)
ϕ_{cap} amortised capital cost of the base unit (US$/day)
ϕ_{op} annualised operating cost (US$/day)
ϕ_T total annualised cost (US$/day)

Subscript
c cold stream/internal
cl clean
coat coating/coated
f fouling layer
h hot stream/external
i at the interface
in inlet
l liquid
op operating
opt optimal
s solubility
wall tube wall

REFERENCES

Bansal, B., Chen, X.D. and Müller-Steinhagen, H., 2008, Analysis of 'classical' deposition rate law for crystallisation fouling. *Chem. Eng. Process.*, Vol. 47, pp. 1201–1210.

Bergman, T., Incropera, F., 2011, Fundamentals of Heat and Mass Transfer, Wiley, New York.

Bott, T.R., 1997, Aspects of crystallization fouling, *Exp. Therm. Fluid Sci*. Vol 14(96), pp. 356–360.

Coletti, F., Ishiyama, E. M. and Paterson, W., 2010, Impact of deposit aging and surface roughness on thermal fouling: distributed model. *AIChE J.*, Vol. 56(12), pp. 3257–3273.

Epstein, N., 1994, A model of the initial chemical reaction fouling rate for flow within a heated tube, and its verification, *Proc. 10th International Heat Transfer Conference*, Brighton, UK.

Fryer, P.J. and Slater, N.K.H., 1985, A direct simulation procedure for chemical reaction fouling in heat exchangers, *Chem. Eng. J.*, Vol. 31(2), pp. 97-107.

Geddert, T., Bialuch, I., Augustin, W. and Scholl, S., 2009, Extending the induction period of crystallization fouling through surface coating, *Heat Trans. Eng.*, Vol. 30(10–11), pp. 868–875.

Gomes da Cruz, L., Ishiyama, E.M., Boxler, C., Augustin, W.A., Scholl, S. and Wilson, D.I., 2015, Value pricing of surface coatings for mitigating heat exchanger fouling, *Food Bioprod. Proc.*, Vol. 93, pp. 343–363.

Helalizadeh, A., Müller-Steinhagen, H. and Jamialahmadi, M., 2000, Mixed salt crystallisation fouling, *Chem. Eng. Process.*, Vol. 39, pp. 29–43.

Hewitt, G.F. and Pugh, S.J., 2007, Approximate design and costing methods for heat exchangers. *Heat Trans. Eng.*, Vol. 28(2), pp. 76–86.

Ishiyama, E.M., Paterson, W.R. and Wilson, D.I., 2008, Thermo-hydraulic channelling in parallel heat exchangers subject to fouling. *Chem. Eng. Sci.*, Vol. 63(13), pp. 3400–3410.

Ma, R.S.T., and Epstein, N., 1981, Optimum cycles for falling rate processes, *Can. J. Chem. Eng.*, Vol. 59(5), pp. 631-633.

Magens, O.M., Ishiyama, E.M., and Wilson, D.I., 7 - 2015, Quantifying the 'implementation gap' for antifouling coatings. *Proc. 3rd Sustainable Thermal Energy Management Conference*, Newcastle upon Tyne, UK

Mayer, M., Augustin, W. and Scholl, S., 2012, Adhesion of single crystals on modified surfaces in crystallization fouling, *J. Cryst. Growth*, Vol. 361(1), pp. 152–158.

Müller-Steinhagen, H. and Zhao, Q., 1997, Investigation of low fouling surface alloys made by ion implantation technology. *Chem. Eng. Sci.*, Vol. 52(19), pp. 3321–3332.

Mullin, J.W., 2001, Crystallization, Butterworth-Heinemann, Oxford.

Mwaba, M.G., Golriz, M.R. and Gu, J., 2006, A semi-empirical correlation for crystallization fouling on heat exchange surfaces, *Appl. Therm. Eng.*, Vol. 26, pp. 440–447.

Pääkkönen, T.M., Riihimäki, M., Simonson, C.J., Muurinen, E. and Keiski, R.L., 2015, Modeling $CaCO_3$ crystallization fouling on a heat exchanger surface – Definition of fouling layer properties and model parameters. *Int. J. Heat Mass Transfer*, Vol. 83, pp. 84–98.

Press, W.H., Teukolsky, S.A., Flannery, B.P. and Vetterling, W.T., 1986, Numerical recipes: The art of scientific computing, Cambridge University Press, New York.

VDI e.V., 2010, VDI Heat Atlas, Springer, Berlin.

Zhao, Q., Liu, Y., Müller-Steinhagen, H. and Liu, G., 2002, Graded Ni–P–PTFE coatings and their potential applications. *Surf. Coat. Technol.*, Vol. 155(2-3), pp. 279–284.